Temporal codes provide additional category-related information in object category decoding: a systematic comparison of informative EEG features

Hamid Karimi-Rouzbahani[1,2]*, Mozhgan Shahmohammadi[3], Ehsan Vahab[4], Saeed Setayeshi[5], Thomas Carlson[6]

[1]Perception in Action Research Centre and Department of Cognitive Science Macquarie University, Australia

[2]Department of Computing, Macquarie University, Australia

[3]Department of Computer Engineering, Central Tehran Branch, Islamic Azad University, Iran

[4]Department of Computer and Information and Technology Engineering, Qazvin Branch, Islamic Azad University, Iran

[5]Department of Medical Radiation Engineering, Amirkabir University of Technology, Iran

[6]School of Psychology, University of Sydney, Australia

* to whom correspondence should be addressed.

Abstract

Humans are remarkably efficent at recognizing objects. Understanding how the brain performs object recognition has been challenging. Our understanding has been advanced substantially in recent years with the development of multivariate pattern analysis or brain decoding methods. Most start-of-the-art decoding procedures, make use of the mean signal activation to extract object category information, which overlooks temporal variability in the signals. Here, we studied category-related information in 30 mathematically different features from the electroencephalography (EEG; the largest set ever) across three independent and highly-varied datasets using multi-variate pattern analyses. While the event-related potential (ERP) components of N1 and P2a were among the most informative features, the informative original signal samples and Wavelet coefficients, down-sampled through principal component analysis, outperformed them. Informative features showed more pronounced effects in the Theta frequency band, which has been shown to support feed-forward processing of visual information. Correlational analyses showed that the features which provided the most information about object categories, could predict participants' performance (reaction time) more accurately than the less informative features. These results provide researchers with new avenues to study how the brain encodes object category information and how we can read out object category to study the temporal dynamics of the neural code.

Keywords

object category processing; multivariate pattern analysis; decoding; EEG; feature extraction

Introduction

How does the brain encode information about visual object categories? This question has been studied for many years using different neural recording techniques including invasive single-cell electrophysiology (Hung et al., 2005), electrocorticography (ECoG; Majima et al., 2014; Watrous et al., 2015; Rupp et al., 2017; Lie et al., 2009; Miyakawa et al., 2018; Liu et al., 2009), and non-invasive methods such as functional Magnetic Resonance Imaging (fMRI; Haxby et al., 2001), magnetoencephalography (Contini et al., 2017; Carlson et al., 2013) and electroencephalography (EEG; Kaneshiro et al., 2016; Simanova et al., 2010) or a combination of them (Cichy et al., 2014). Despite the recent successes in neuroimaging in "reading-out" or "decoding" neural representations of semantic object categories, it is unclear whether contemporary decoding analyses leverage the main feature in which recorded neural activity reflects object category information. These analyses generally rely on the signal 'mean' amplitude, which although informative, but might be a sub-optimal feature to decode the object category information from. The use of this sub-optimal feature might thus hide the true spatiotemporal dynamics of categorical object encoding in the brain, which is still debated in cognitive neuroscience (Majima et al., 2014; Karimi-Rouzbahani et al., 2017a; Behroozi et al. 2016). Here, we characterize the most informative features or features of the recorded brain activity, which provide object category information, and evaluate their relevance by measuring how well each feature explains behavioral object recognition performance.

Many neuroimaging studies (i.e. fMRI, MEG and EEG) have studied the neural codes of object categories through the use of multi-variate pattern analysis (MVPA; also called decoding). MVPA incorporates activations across multiple recording sites (i.e. sensors in M/EEG or brain volumes in fMRI) to detect subtle but widespread differences between patterns of activity across conditions (e.g. object categories). These differences might not be detectable when comparing single-sensor univariate brain activations (Norman et al., 2006; Grootswagers et al., 2017), such as when comparing conventional event-related potentials (ERPs) in EEG (Ambrus et al., 2019). While fMRI provides millimeter-scale spatial resolution allowing us to localize the brain areas involved in object category processing (Haxby et al., 2001), the recorded activations are usually modelled using generalized linear regression techniques for both univariate and multivariate analyses. This statistical modelling approach, which is a prerequisite step when analyzing evoked activations, removes many critical/relevant temporal variabilities (i.e. potential codes) which have been shown to provide information about object categories when adopting methods with high temporal resolution such as ECoG and EEG (Majima et al., 2014; Karimi-Rouzbahani et al., 2017a).

The temporal precision of MEG and EEG allow us to analyze the temporal variabilities with millisecond resolution. Utilizing the high temporal resolution of M/EEG along with the sensitivity of MVPA/decoding, the communities of neuroscience, machine learning and brain-computer interface (BCI) have gained deeper insights into how we can decode information about object categories from recorded neural activity. Earlier decoding studies have shown that individual amplitude-based ERP components such as N1, P1, P2a and P2b, which refer to arbitrary time windows in signal's time series extracted from 100 to 300 ms post-stimulus onset, could be used to reliably differentiate visual object categories (Chan et al., 2011). Later studies used Linear Discriminant Analysis (LDA) classifiers to discriminate up to four object

categories utilizing the information content of those ERP components (Wang et al., 2012), which were later fused to improve previous decoding accuracies (Qin et al., 2016). However, these studies and others (Taghizadeh-Sarabi et al., 2015; Torabi et al., 2017; Wang et al., 2018) overlook the temporal dynamics of object encoding based on within-trial variations in the signals. To address this issue, researchers repeated the decoding procedure in short (e.g. 4~50 ms) sliding time windows within trials and revealed the dynamical profile of category information within trials, which significantly varied by factors such as task, image presentation time, etc (Karimi-Rouzbahani et al., 2017a; Karimi-Rouzbahani et al., 2017b; Karimi-Rouzbahani et al., 2018; Karimi-Rouzbahani et al., 2019; Grootswagers et al., 2017; Grootswagers et al., 2019). While providing a temporal account for the neural object category processing, these time-resolved decoding studies overlook other possible features of neural activations that could provide additive information or differential dynamics for neural object category processing.

To address this issue, studies have investigated other features of brain activations such as phase (Behroozi et al., 2016; Watrous et al., 2015; Torabi et al., 2017; Wang et al., 2018), signal power across frequency bands (Rupp et al., 2017; Miyakawa et al., 2018; Behroozi et al., 2016), time-frequency features such as Wavelet coefficients (Hatamimajoumerd and Talebpour, 2019; Taghizadeh-Sarabi et al., 2015), inter-electrode correlation (Majima et al., 2014; Karimi-Rouzbahani et al., 2017a), non-linear statistical features (Joshi et al., 2018; Torabi et al., 2017; Stam, 2005). Behroozi et al., (2016) decoded object categories using signal phase patterns in the delta frequency band (i.e. 1-4 Hz). This finding was later investigated by another group using Hilbert transform, but found the information in the theta frequency band (4-8 Hz; Wang et al., 2018). Other studies found that signal power contained significant category-related information (Rupp et al., 2017; Majima et al., 2014; Miyakawa et al., 2018). An ECoG investigation found object category information in the synchronization of low- (~2.5 Hz) and high-frequency (~84 Hz) oscillations (Watrous et al., 2015). A few human and monkey ECoG studies observed that signal power in a wide range of frequency bands carried significant amounts of category information (Majima et al., 2014; Miyakawa et al., 2018), but the information content may be different across frequency bands (Miyakawa et al., 2018). Research has also shown that Wavelet coefficients, which provide spatiotemporal information about signal variations, contain category information (Taghizadeh-Sarabi et al., 2015). Another study showed that, nonlinear statistical features, such as fractal dimensions, Hjorth complexity, and entropy, which measure the complexity of signals as an indicator of its information richness, could discriminate object categories (Torabi et al., 2017; Joshi et al., 2018). These feature-based studies, however, were done on whole-trial time windows, thus they provided no insight into temporal dynamics.

Together, these extant literature leaves three unanswered questions about the neural decoding of object categories. First, which features of the recorded signals are most informative about object categories? Specifically, while several of the above studies have compared multiple features, they focused on specific feature types such as ERP components (Chan et al., 2011), Wavelet (Taghizadeh-Sarabi et al., 2015) or non-linear features (Torabi et al., 2016), limiting our understanding of how different feature types compare to one another. Moreover, some features (e.g. signal power (Behroozi et al., 2016 vs. Wang et al., 2018), inter-electrode correlation (Majima et al., 2014 vs. Karimi-Rouzbahani et al., 2017a) have shown discrepancy across studies/datasets. This suggest that their results might have

been driven by category-irrelevant task features such as attentional load or task demands, which can modulate the neural activity to a greater level than that evoked by the stimulus (Karimi-Rouzbahani et al., 2019; Karimi-Rouzbahani et al., 2020b). Therefore, a wider set of features and datasets should be evaluated to reach more generalizable conclusions.

Second, what are the temporal dynamics of object category decoding when using distinct features of brain activations? Very few studies have investigated the role of features, other than mean activations, across the time course of trials (Majima et al., 2014; Stewart et al., 2014; Karimi-Rouzbahani et al., 2017a). An ECoG study by Majima et al., 2014 showed that inter-electrode correlation of time samples carried more categorical information than signal power and phase features in 100 and 300-ms wide sliding time windows. We have recently found that inter-electrode correlation of time samples carried categorical object information, but it was much less informative than the signal variance within 50 ms sliding time windows (Karimi-Rouzbahani et al., 2017a). These studies show that features, other than mean, that have temporal profiles can potentially provide additional information about neural category processing.

Third, which features of brain activations explain behavioral recognition performance? A major open question in neuroimaging is whether the information that is extracted from neural activity is relevant or is just epiphenomenal to the target conditions. To answer this question, recent efforts have tried to explain behavioral performance using the neural decoding results on the same experiment (Williams et al., 2007; Grootswagers et al., 2018; Woolgar et al., 2019). These studies found that the decoding accuracy obtained by analyzing mean signal activations can predict the behavioral performance in object recognition (Ritchie, et al., 2015). However, it has remained unknown how (if at all) the decoding accuracies obtained from other activation features can explain more variance in behavioral performance.

To address these questions, we re-implemented a set of 30 features from the literature- as the biggest set of features ever evaluated for decoding of object category information in EEG- and evaluated their information about object categories from neural activity on the whole trial as well as sliding time windows. We evaluated the features across three datasets, which varied in many parameters including the image set, task, and paradigm. This allowed us to obtain more generalizable results about the role of each feature in category decoding and explaining behavioral object recognition performance.

Methods

Overview of Datasets

We chose three previously published EEG datasets for this study, which differed across a wide range of parameters including the recording set-up (e.g. amplifier, number of electrodes, preprocessing steps, etc.), characteristics of the image-set (e.g. number of categories and exemplars within each category, colorfulness of images, etc.), paradigm and task (e.g. presentation length, order and the participants' task;

Table 1). All three datasets previously successfully provided object category information from electrical brain activity using multivariate decoding methods.

Dataset 1. We have previously collected dataset 1 while participants were briefly (i.e. 50 ms) presented with gray-scale images from four synthetically-generated 3D object categories (Karimi-Rouzbahani et al., 2017a). The objects underwent systematic variations in scale, positional periphery, in-depth rotation and lighting conditions, which made their perception difficult, especially in extreme variation conditions. Randomly ordered stimuli were presented in consecutive pairs (Figure 1, top row). The participants' task was unrelated to object categorization- they pressed one of two pre-determined buttons to indicate if the fixation dots, superimposed on the first and second stimuli, were the same/different color (2-alternative forced-choice).

Dataset 2. We have collected dataset 2 in an active experiment, in which participants pressed a button if the presented object image was from a target category (go/no-go), which was cued at the beginning of each block of 12 stimuli (Karimi-Rouzbahani et al., 2019; Figure 1, middle row). The object images, which were cropped from real photographs, were part of the well-stablished benchmark image set for object recognition developed by Kiani et al., (2007), which has been previously used to extract object category information from both human and monkey brain using MEG (Cichy et al., 2014), fMRI (Cichy et al., 2014; Kriegeskorte et al., 2008) and single-cell electrophysiology (Kriegeskorte et al., 2008; Kiani et al., 2007).

Dataset 3. We also adopted another dataset (dataset #3) which was not collected in our lab. This dataset was collected by Kaneshiro et al., (2015) on 6 sessions for each participant, from which we used the first session only, as it could represent the whole dataset- other sessions were repetitions of the first session and aimed at increasing the signal to noise ratio by repeating the presentation of the same stimuli. The EEG data was collected during passive viewing (participants had no task; Figure 1, bottom row) of 6 categories of objects with stimuli chosen from Kiani et al. (2007) as explained above. We used a pre-processed (i.e. band-pass-filtered in the range 0.03 to 50 Hz) version of the dataset which was available online[1].

[1] https://purl.stanford.edu/tc919dd5388

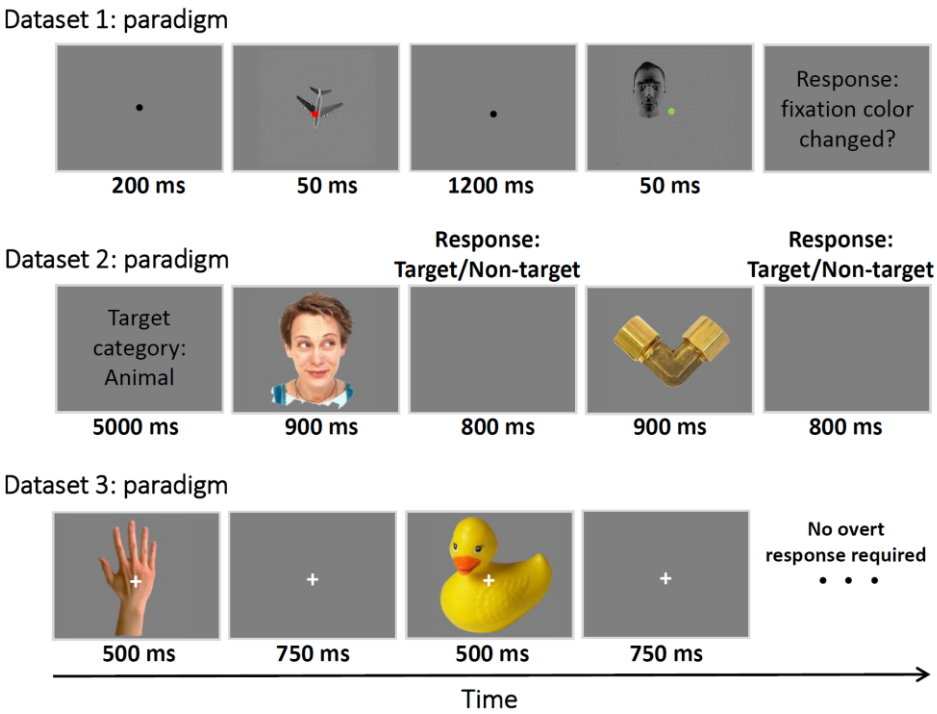

Figure 1. Paradigms of the datasets used in this study. Dataset 1 (top row) presented two consecutive object images with a fixation dot. Participants' task was to indicate if the fixation dot was the same or different colors across the object images (passive task). Dataset 2 (middle row) presented objects from the target and non-target categories in sequences of 12 images. Participant's task was to indicate, for each image, if it was from the target/non-target category (active task). Dataset 3 (bottom row), presented sequences of object images from 6 different categories. Participants did not have any specific task, except for looking at the center of object images (no overt task). Please see the details of the datasets in the relevant references cited in Table 1.

All three datasets were collected at a sampling rate of 1000 Hz. For datasets 1 and 2, only the trials which led to correct responses by participants, were used in the analyses. Each dataset consisted of data from 10 participants. Each object category in each dataset included 12 exemplars. To make the three datasets as consistent as possible, we pre-processed them differently from their original papers. Specifically, the band-pass filtering range of dataset 3 was 0.03 to 50 Hz, and we did not have access to the raw data to increase the upper bound to 200 Hz. Datasets 1 and 2 were band-pass-filtered in the range from 0.03 to 200 Hz. We used finite-impulse-response filters with 12 dB roll-off per octave for band-pass filtering of datasets 1 and 2 and when evaluating the sub-bands of the three datasets. We did not remove artifacts (e.g. eye-related and movement-related) from the datasets, as we and others have shown that sporadic artifacts have minimal effect in MVPA (Grootswagers et al., 2017). To increase signal to noise ratios in the analyses, each unique stimulus had been presented to the participants 3, 6 and 12 times in datasets 1, 2, 3, respectively. Trials were defined in the time window from 200 ms before to 1000 ms after the stimulus onset to cover most of the range of event-related neural activations. For more information about each dataset see Table 1 and references to their original publications.

Table 1. Details of the three datasets used in the study.

	Dataset	# electrodes	Band-pass filtering range	Notch filtering	# object categories	Stimulus presentation time	Stimulus size (periphery)	Task
1	Karimi-Rouzbahani et al., 2017a	31	0.03-200 Hz	50 Hz	4	50 ms	2~13.5° (0.7~8.8°)	Color matching (passive)
2	Karimi-Rouzbahani et al., 2019	31	0.03-200 Hz	50 Hz	4	900 ms	8° × 8°	Object category detection (active)
3	Kaneshiro et al., 2017	124	0.03-50 Hz	No	6	500 ms	7.0° × 6.5°	No task (fixation)

Features

Moment features

Mean

Mean, which is the first signal moment, refers to the signal's sample mean. Sample mean is the average value of a signal which provides an estimation of the time series' mean value calculated as:

$$\bar{x} = \frac{1}{N}\sum_{t=1}^{N} x_t \quad (1)$$

where $\bar{x}$ is the mean of the N time samples contained in the time series. x_t refers to the sample value at time point t. Signal's mean is the measure most widely used in quantifying neural activations, in both non-invasive and invasive neural recording, in limited time windows and across the whole time series (Grootswagers et al., 2017; Karimi-Rouzbahani et al., 2019).

Median

Compared to the signal's mean, Median is less susceptible to outliers in the time series, which might not come from neural activations but rather from the recording hardware, preprocessing, etc. Provided that the signal probability distribution is P, signal median, m, is calculated so that it meets the following conditions: $P(x > m) \geq \frac{1}{2}$ and $P(x \leq m) \geq \frac{1}{2}$ (2)

Variance

Variance, which is the second signal moment, is a measure of variability in the signal and has been shown to provide information about object categories and sensory visual inputs in neural activity (Karimi-Rouzbahani et al., 2017a). Variance is calculated as:

$$\sigma^2 = \frac{1}{N}\sum_{t=1}^{N}(x_t - \bar{x})^2 \quad (3)$$

Skewness

Skewness, which is the third signal moment, measures the degree of asymmetry in the signal's probability distribution. In symmetric distribution (i.e. when samples are symmetrically around the mean) skewness is zero. Positive and negative skewness indicates right- and left-ward tailed distribution, respectively. Skewness is calculated as:

$$\gamma_1 = \frac{1}{N}\sum_{t=1}^{N}\left(\frac{x_t-\bar{x}}{\sigma}\right)^3 \quad (4)$$

Kurtosis

Kurtosis reflects the degree of 'tailedness' or 'flattedness' of the signal's probability distribution. Accordingly, the more heaviness in the tails, the less value of Kurtosis. It is the fourth standardized moment of the signal defined as:

$$Kurt = \frac{1}{N}\sum_{t=1}^{N}\left(\frac{x_t-\bar{x}}{\sigma}\right)^4 \quad (5)$$

There can potentially be many cases in which simple statistical measures such as mean, variance, skewness and kurtosis do not provide distinct values for distinct time series (e.g. A: 10, 20, 10, 20, 10, 20, 10, 20 vs. B: 20, 20, 20, 10, 20, 10, 10, 10, for both of which the four above-mentioned moments provide equal values). Therefore, we need more complicated features which enable us to discriminate distinct time series. In the following, we briefly explain other statistical features that we used in our analyses.

Complexity features and ERP components

Lempel-Ziv complexity (LZ Cmplx)

Lempel-Ziv is a compression technique, which can measure the complexity of a signal time series (Lempel et al., 1976). Basically, the algorithm counts the number of unique sub-sequences within a larger binary sequence. Accordingly, a sequence of samples with a certain regularity does not lead to a large LZ complexity. However, the complexity generally grows with the length of the sequence and its irregularity. The algorithm has different implementations, and we used the implementation by Quang Thai [2] implemented based on "exhaustive complexity" which is considered to provide the lower limit of the complexity as explained by Lempel et al. (1976). We used the signal median as a threshold to convert the signals into binary sequences for the calculation of LZ complexity. The LZ complexity provided a single value for each signal time series.

Fractal dimension

In signal processing, fractal is an indexing technique which provides statistical information determining the complexity of how data are organized in time series. A higher fractal value indicates more complexity of a sequence as reflected in more nesting of repetitive sub-sequences at all scales. Fractal dimensions

[2] https://www.mathworks.com/matlabcentral/fileexchange/38211-calc_lz_complexity

are widely used to measure two important attributes: self-similarity and the shape of irregularity. In this study, we implemented two methods for the calculation of fractal dimensions of EEG time series, which have been previously used to extract information about object categories (Torabi et al., 2017).

- **Higuchi's fractal dimension (Higuchi FD)**

In this method (Higuchi et al., 1988), a set of sub-sequences x_k^m is generated in which k and m refer to the step size and initial value, respectively. Then, the length of this fractal dimension is calculated as:

$$L_k^m = \frac{\left\{\left[\sum_{i=1}^{\left[\frac{N-m}{k}\right]} \left|x_{(m+ik)} - x_{(m+(i-1).k)}\right|\right] \frac{N-1}{\left[\frac{N-m}{k}\right].k}\right\}}{k} \tag{6}$$

where $\frac{N-1}{\left[\frac{N-m}{k}\right].k}$ is the normalization factor. The length of the fractal curve at step size of k is calculated by averaging k sets of L_k^m. Finally, the resultant average will be proportional to k^{-D} where D is the fractal dimension. We set the free parameter of k equal to half the length of signal time series.

- **Katz's fractal dimension (Katz FD)**

We also calculated fractal dimension using Katz's method (Katz, 1988) as it showed a significant amount of information about object categories in a previous study (Torabi et al., 2017). The fractal dimension (D) is calculated as:

$$D = \frac{log_{10}(\frac{L}{a})}{log_{10}(\frac{d}{a})} = \frac{log_{10} r}{log_{10}\left(\frac{d}{L}\right) + log_{10} r} \tag{7}$$

where L and a refer to the sum and average of the consecutive signal samples, respectively. Also d refers to the maximum distance between first sample of the signal and i^{th} sample of the signal which has the maximum distance from first sample as:

$$L = \sum_{i=2}^{n} |x_i - x_{i-1}| \tag{8}$$

$$d = max(distance(1, i)) \tag{9}$$

$$r = L/a \tag{10}$$

Hurst exponent (Hurst Exp)

Hurst exponent is widely used to measure the long-term memory in a time-dependent random variable such as biological time series (Racine, 2011). In other words, it calculates the degree of dependence and operates like an autocorrelation function over time. Hurst values between 0.5 and 1 suggest consecutive appearance of high signal values on large time scales while values between 0 and 0.5 suggest frequent switching between high and low signal values. Values around 0.5 suggest no specific patterns among samples of a time series. It is defined as an asymptotic behavior of a rescaled range as a function of the time span of the time series defined as:

$$E\left[\frac{\max(z_1,z_2,\ldots,z_N)-\min(z_1,z_2,\ldots,z_N)}{\sqrt{\frac{1}{N}\sum_{t=1}^{N}(x_t-\bar{x})^2}}\right] = C.N^H \; as \; N \rightarrow \infty \tag{11}$$

$$z_t = \sum_{i=1}^{t} y_i \; ; t = 1, \ldots, N \tag{12}$$

$$y_t = x_t - \bar{x} \tag{13}$$

where E is the expected value, C is a constant and H is the Hurst exponent (Racine, 2011). We used the open-source implementation of the algorithm[3], which has also been used previously for the decoding of object category information in EEG (Torabi et al., 2017).

Entropy

Entropy can measure the perturbation in time series. A higher value for entropy suggests a higher irregularity in the given time series. Precise calculation of entropy usually requires considerable number of samples and is also sensitive to noise. Here we used two methods for the calculation of entropy, each of which has its advantages over the other.

- **Approximate entropy (Apprx Ent)**

Approximate entropy was initially developed to be used for medical data analysis (Pincus and Huang, 1992), such as heart rate, and then was extended to other areas such as brain data analysis. It has the advantage of requiring a low computational power which makes it perfect for real-time applications on low sample sizes (N<50). However, the quality of this entropy method is impaired on lower length of the data. We used an open-source code[4] for calculating approximate entropy. We set the embedded dimension and the tolerance parameters to 2 and 20% of the standard deviation of the data, respectively.

- **Sample entropy (Sample Ent)**

Sample entropy is frequently used to calculate regularity of biological signals (Richman et al., 2000). It has two main advantages to the approximate entropy: it is less sensitive to the length of the data and is simpler to implement. However, it does not focus on self-similar patterns in the data. We used the Matlab's 'entropy' function for the implementation of this feature. See (Richman et al., 2000) for the details of the algorithm.

Autocorrelation (Autocorr)

Autocorrelation determines the degree of similarity between the samples of a given time series and a time-lagged version of the same series. It detect periodic patterns in signal time series. Autocorrelation is calculated as:

[3] https://www.mathworks.com/matlabcentral/fileexchange/9842-hurst-exponent

[4] https://www.mathworks.com/matlabcentral/fileexchange/32427-fast-approximate-entropy

$$R(\tau) = \frac{1}{(N-\tau)\sigma^2}\sum_{t=1}^{N-\tau}(x_t - \bar{x})(x_{t+\tau} - \bar{x}) \quad (14)$$

where τ indicates the number of lags in samples of the shifted signal. A positive value for autocorrelation indicates a strong relationship between the original time series and its shifted version, whereas a negative autocorrelation refers to an opposite pattern between them. Zero autocorrelation indicates no relationship between the original time series and its shifted version. In this study, we extracted autocorrelations for 30 consecutive lags ([τ=1, 2, . . ., 30]) used their average in classification. Please note that each lag refers to 1 ms as the data was sampled at 1000 Hz.

Hjorth parameters

Hjorth parameters are descriptors of statistical properties of signals introduced by Hjorth (1970). These parameters are widely used in EEG signal analysis for feature extraction across a wide set of applications including visual recognition (Joshi et al., 2018; Torabi et al., 2017). These features consist of Activity, Mobility and Complexity as defined below. As the Activity parameter is equivalent to a signal's variance, which we already had in the analyses, we did not use it twice.

- **Hjorth complexity (Hjorth Cmp)**

It determines the variation in signal's frequency by quantifying the similarity between the signal and a pure sine wave leading to a value of 1 in case of perfect match. In other words, values around 1 suggest lower complexity for a signal. It is calculated as:

$$Complexity = \frac{Mobility\ (\frac{dx_t}{dt})}{Mobility\ (x_t)} \quad (15)$$

- **Hjorth mobility (Hjorth Mob)**

It determines the proportion of standard deviation of the power spectrum as is calculated below, where var refers to the signal variance.

$$Mobility = \sqrt{\frac{var(\frac{dx_t}{dt})}{var(x_t)}} \quad (16)$$

ERP components (N1, P1, P2a and P2b)

An ERP is a measured brain response to a specific cognitive, sensory or motor event that provides an approach to study the correlation between the event and neural processing. According to the latency and amplitude, ERP is split into specific sub-windows called components. Here, we extracted ERP components by calculating mean of signals in specific time windows to obtain the P1 (80 to 120 ms), N1 (120 to 200 ms), P2a (150 to 220 ms) and P2b (200 to 275 ms) components, which were shown previously to provide significant amounts of information about visual object and face processing (Jadidi et al., 2016; Wang et al., 2012).

Frequency-domain features

Signal power (Signal Pw)

Power spectrum density (PSD) represents the intensity or the distribution of the signal power into its constituent frequency components. Studies have shown the associations between aspects of visual perception and certain frequency bands (Rupp et al., 2017). According to the Fourier analysis, every signal can be broken into separate frequency components or a spectrum of frequencies in a specific frequency range. Here, we calculated signal power using the PSD according to equation (17).

$$\tilde{S}_{xx}(w) = \frac{(\Delta t)^2}{T} \left| \sum_{n=1}^{N} x_n e^{-iwn\Delta t} \right|^2 \quad (17)$$

where $x_n = x_{n\Delta t}$ is signal which has been sampled at a rate of $T = \frac{1}{\Delta t}$ and w is the frequency at which the signal power is calculated.

Mean frequency (Mean Freq)

Mean frequency is the average of all frequency components available in a signal. Assume a signal consisting of two frequency components of f_1 and f_2. The mean frequency of the signal would be $f_{mean} = \frac{f_1+f_2}{2}$. Generally, the mean frequency is calculated using the following formula:

$$f_{mean} = \frac{\sum_{i=0}^{n} l_i f_i}{\sum_{i=0}^{n} l_i} \quad (18)$$

where n is the number of splits of the PSD, f_i and l_i are the frequency and the intensity of the PSD in its ith slot, respectively. It was calculated using Matlab's 'meanfreq' function.

Median frequency (Med Freq)

Median frequency is the median normalized frequency of the power spectrum of a time-domain signal. It is calculated similarly to the signal median in the time domain, however, here the values are the power intensity in different frequency slots of the PSD. It was calculated using Matlab's 'medfreq' function.

Average frequency (Avg Freq)

It calculates the number of times the signal passes zero. In other words, it measures the zero-crossing rate of the signal. Note that each trial is baselined according to the average of the same trial in the last 200 ms immediately before the stimulus onset. We calculated the zero crossing rate on the post-stimulus time span from the time point of 0 to 1000 ms.

Spectral edge frequency (SEF 95%)

SEF is a common feature used in monitoring the depth of anesthesia and stages of sleep using EEG (Iranmanesh and Rorigues-Villegas, 2017). It measures the frequency which covers X percent of the PSD. X is usually set between 75 to 95%. Here we set X to 95%.

Power and Phase at median frequency (Pw MdFrq and Phs MdFrq)

Apart from the median frequency itself, the power and phase of the signal at this frequency have been shown to contain information about aspects of perception (Joshi et al., 2018; Jadidi et al., 2016). Therefore, we calculated the power and phase of the frequency-domain signals at the median frequency as features.

Multi-valued features

The multi-valued features explained below refer to features which provided more than a single value for every time window of analysis (i.e. 50 ms or the whole trial). These multi-valued features, were reduced in dimension to one per electrode per time window before conducting the decoding analyses, to allow for direct comparison with single-valued features explained above.

Inter-electrode correlation (Cros Cor)

Inter-electrode correlation, which is basically cross-correlation, is a measure of similarity between two different signals, here, from different electrodes. A few recent studies have used this feature in decoding object category information from brain activations and have provided evidence that the relationship of between activity patterns of different electrodes can provide information about object categories (Majima et al., 2014; Karimi-Rouzbahani et al., 2017a). It is calculated as:

$$R_{xy} = \frac{1}{N\sigma_x\sigma_y}\sum_{t=1}^{N}(x_t - \bar{x})(y_t - \bar{y}) \quad (19)$$

where x and y refer to the signals obtained from electrodes x and y, respectively. We calculated the cross-correlation between every given electrode and all the other electrodes before finally averaging them to obtain a single value per electrode. Therefore, for the datasets with 31 (i.e. datasets 1 and 2) and 128 (i.e. dataset 3) electrodes, we obtained 30 and 127 inter-electrode correlations per electrode.

Wavelet transform (Wavelet)

Wavelet transform provides a spatiotemporal representation of the primary frequency components of a specific signal and their temporal locations. It passes the signal time series through digital filters (Guo et al., 2009; equation (20)), using the convolution operator, each of which are adjusted to extract a specific frequency at a specific time:

$$y_n = (x * g) = \sum_{k=-\infty}^{+\infty} x_k g_{n-k} \quad (20)$$

where g is the digital filter and $*$ is the convolution operator. This filtering procedure is repeated for several rounds (levels) filtering low- (approximations) and high-frequency (details) components of the signal to provide more fine-grained information into the constituent components of it. This can lead to coefficients which can potentially discriminate signals evoked by different conditions, therefore enabling the decoding of object categories as it has been the case in many recent studies (Taghizadeh-Sarabi et al.,

2015; Torabi et al., 2017). As in a previous study (Taghizadeh-Sarabi et al., 2015), and to make the number of Wavelet features comparable in number to the signal samples (which were 1000 after the stimulus onset), we used detail coefficients at five levels $D1, \ldots, D5$ as well as the approximate coefficients at level 5, $A5$. This led to 1015 features in the whole-trial and 57 in the 50 ms sliding time windows, respectively. We used the '*Symlet2'* basis function for our Wavelet transformations as implemented in Matlab.

Hilbert transform (Hilb Amp and Hilb Phs)

In signal processing, Hilbert transform is described as a mapping function that takes a function $x(t)$ of a real variable, and using convolution with the function, $\frac{1}{\pi t}$, produces another function of a real variable $H(u)(t)$ as:

$$H(u)(t) = \frac{1}{n}\int_{-\infty}^{+\infty} \frac{u(\tau)}{t-\tau} d\tau \quad (21)$$

where $H(u)(t)$ is a frequency-domain representation of the signal, which has simply shifted all the components of the input signal by $\frac{\pi}{2}$. In the current study, Hilbert transform was applied on every trial (1000 samples) or 50 ms sliding time windows, which produced one amplitude and one phase component per sample, so 1000 and 50 for the whole-trial and 50 ms sliding time windows, respectively. We used the amplitude and phase components separately to discriminate object categories in the decoding analyses. This technique has recently shown success in decoding visual letter information from EEG signals (Wang et al., 2018).

Signal samples (Samples)

We also used the post-stimulus signal samples (i.e. 1000 or 50 samples for the whole-trial and sliding time windows, respectively) to decode object category information without any feature extraction. This allowed us to compare the information content of the extracted features with the original signal samples to see if the former provided any extra information.

Multivariate pattern analysis (MVPA)

We used MVPA to extract information about object categories from the EEG datasets. Basically, MVPA, which has dominated neuroimaging studies recently (Grootswagers et al., 2017), utilizes within- and cross-condition similarity/distance to determine the amount of information when contrasting those conditions. We used linear discriminant analysis (LDA) classifiers to measure the information content across all possible pairs of conditions (i.e. object categories) in each dataset throughout our MVPA analyses. This classifier has been shown to be robust (Grootswagers et al., 2017) and was around 30 times faster to train in our initial analyses compared to the more complex classifier of support-vector machine (SVM), which provided visually comparable results. We used a 10-fold cross-validation procedure in which we trained the classifier on 90% of the data and tested it on the left-out 10% of the data, repeating the procedure 10 times until all trials from the pair of categories participate once in the training and once in the testing of the classifiers. We repeated the MVPA across all possible pairs of

categories within each dataset, which were 6, 6 and 15 pairs for datasets 1, 2 and 3, which consisted of 4, 4 and 6 object categories, respectively. Finally, we averaged the results across all combinations and reported them as the average decoding for each participant.

In the whole-trial analyses, we extracted the above-mentioned features from the 1000 data samples after the stimulus onset (i.e. from 1 to 1000 ms). In the time-resolved analyses, we extracted the features from 50 ms sliding time windows in steps of 5 ms across the time course of the trial (-200 to 1000 ms relative to the stimulus onset time). Therefore, in time-resolved analyses, the MVPA results at each time point reflect the data for the 50 ms window around the time point, from -25 to +24 ms relative to the time point. Time-resolved analyses allowed us to evaluate the evolution of object category information across time as captured by different features.

Dimensionality reduction

The multi-valued features explained above resulted in more than a single feature value per trial per sliding time window (e.g. inter-electrode correlation, wavelet, Hilbert amplitude and phase and signal samples), which could bias the results when comparing the them with those obtained from single-valued features. To avoid that, we used principle component analysis (PCA) to reduce the number of values in the multi-valued features to one per electrode per time window, which was the number of values for all the other (single-valued) features. Specifically, the data matrix before dimension reduction, had a dimension of n rows by $e \times f$ columns where n, e and f were the number of trials in the dataset (consisting of all trials from all categories), the number of electrodes and the number of values from obtained from a given feature (concatenated in columns), respectively. As $f = 1$ for the single-valued features, for the multi-valued features, we only retained the e most informative columns that corresponded to the e eigen values with highest variance and removed the other columns using PCA. Therefore, we reduced the dimension of the data matrix to $n \times e$ which was equal between single- and multi-valued features and used the resulting data matrix for MVPA. This means that, for the multi-valued features, we only maintained the most informative value of the extracted values from each feature and electrode (i.e. the one with the most variance). To avoid potential leakage of information from testing to training (Pulini et al., 2019), we applied the PCA algorithm on the training data (folds) only and used the training PCA parameters (i.e. eigen vectors and means) for both training and testing sets for dimension reduction in each cross-validation run separately. Note that, we did not reduce the dimension of the neural space (columns in the final data matrix) to below the number of electrodes "e" (as in Hatamimajoumerd et al., 2019) as we were interested in qualitatively comparing our results with the vast literature currently using MVPA with all sensors (Grootswagers et al., 2017; Karimi-Rouzbahani et al., 2017a; Cichy et al., 2014, etc.).

Statistical analyses

Bayes factor analysis

To determine the evidence for the null and the alternative hypotheses, we used Bayes analyses as implemented by Bart Krekelberg[5] based on Rouder et al. (2012). We used standard rules of thumb for interpreting levels of evidence (Lee and Wagenmakers, 2014; Dienes, 2014): Bayes factors of >10 and <1/10 were interpreted as strong evidence for the alternative and null hypotheses, respectively, and >3 and <1/3 were interpreted as moderate evidence for the alternative and null hypotheses, respectively. We considered the Bayes factors which fell between 3 and 1/3 as suggesting insufficient evidence either way.

In the whole-trial decoding analyses, we asked whether there was a difference between the decoding values obtained from all possible pairs of features and also across frequency bands within every feature. Accordingly, we performed the Bayes factor unpaired *t-test* and calculated the Bayes factor as the probability of the data under alternative (i.e. difference) relative to the null (i.e. no difference) hypothesis between all possible pairs of features and also across frequency bands within every feature and dataset separately. The same procedure was used to evaluate evidence for difference (i.e. alternative hypothesis) or no difference (i.e. null hypothesis) in the maximum and average decoding accuracies, the time of maximum and above-chance decoding accuracies across features for each dataset separately.

We also evaluated evidence for the alternative of above-chance decoding accuracy vs. the null hypothesis of no difference from chance. For that purpose, we calculated the Bayes factor between the distribution of actual accuracies obtained and a set of 1000 random accuracies obtained by randomizing the class labels across the same pair of conditions (null distribution) on every time point (or only once for the whole-trial analysis), for each feature and dataset separately.

The priors for all Bayes factor analyses were determined based on Jeffrey-Zellner-Siow priors (Jeffreys, 1961; Zellner and Siow, 1980) which are from the Cauchy distribution based on the effect size that is initially calculated in the algorithm using t-test (Rouder et al., 2012). The priors are data-driven and have been shown to be invariant with respect to linear transformations of measurement units (Rouder et al., 2012), which reduces the chance of being biased towards the null or alternative hypotheses.

Random bootstrapping testing

To evaluate the significance of correlations between decoding accuracies and behavioral reaction times, we calculated the percentage of the actual correlations that were higher (if positive) or lower (if negative) than a set of 1000 randomly generated correlations. These random correlations were obtained by randomizing the order of participants' data in the behavioral reaction time vector (null distribution) on every time point, for each feature separately. The correlation was considered significant if surpassed

[5] https://klabhub.github.io/bayesFactor/

95% of the randomly generated correlations in the null distribution in either positive or negative directions ($p < 0.05$) and the p-values were corrected for multiple comparisons across time.

Results

Which features of the recorded signals are most informative about object categories?

To answer the first question of this study, we compared decoding accuracies in the whole-trial time span across all features and for each dataset separately (Figure 2A, black bars). Not all features could provide strong (BF>10) evidence for above-chance decoding (Figure 2A). There was strong evidence (BF>10) that the four ERP components (i.e. P1, N1, P2a and P2b), and a few multi-valued features consisting of Wavelet, Hilb Phs and Samples provided above-chance decoding. Consistently across the three datasets, there was moderate or strong evidence (BF>3; Figure 2B; black boxes) that most of the ERP components (i.e. N1, P2a and P2b) and multi-valued features (i.e. Wavelet, Hilb Phs and signal samples) provided higher decoding accuracies compared to the rest of the features. Although with lower values, there was also moderate or strong evidence (BF>3) that Mean (dataset 3), Median (dataset 3), Autocor (datasets 1 and 2) and Hurst Exp (dataset 1) provided higher accuracies compared to other features in specific datasets. Dataset 2 showed higher decoding values compared to the other datasets, which can be potentially explained by the active object detection task and longer image presentation time. These results showed that the ERP components (i.e. N1, P2a and P2b) as well as multi-valued features (i.e. Wavelet, Hilb Phs and Samples) are most informative about object categories.

We also compared the decoding accuracies across different frequency sub-bands to compare our results with those from previous studies which reported effects in specific frequency sub-bands such as theta (Behroozi et al., 2016; Bastos et al., 2015). We evaluated the information contents of features in the well-known EEG frequency bands of delta (0.5-4 Hz), theta (4-8 Hz), alpha (8-12 Hz), beta (12-16 Hz) and gamma (>25 Hz) against the broad-band signals, which covered the whole available spectrum after pre-processing (>0.03Hz, Figure 2). We did not calculate the decoding accuracies for any of the frequency-domain features (except Signal pw), as they would be meaningless in limited frequency bands by definition. For Signal Pw, however, we calculated the decoding accuracies as it could be calculated in the time domain. When compared to the broad-band results, a similar pattern of decoding was observed especially in the mid-frequency sub-bands of Theta, Alpha and Beta (Figure 2A) with moderate to strong evidence (BF>3; Figure 2B; red boxes) that ERP components and multi-valued features were the most informative about object categories.

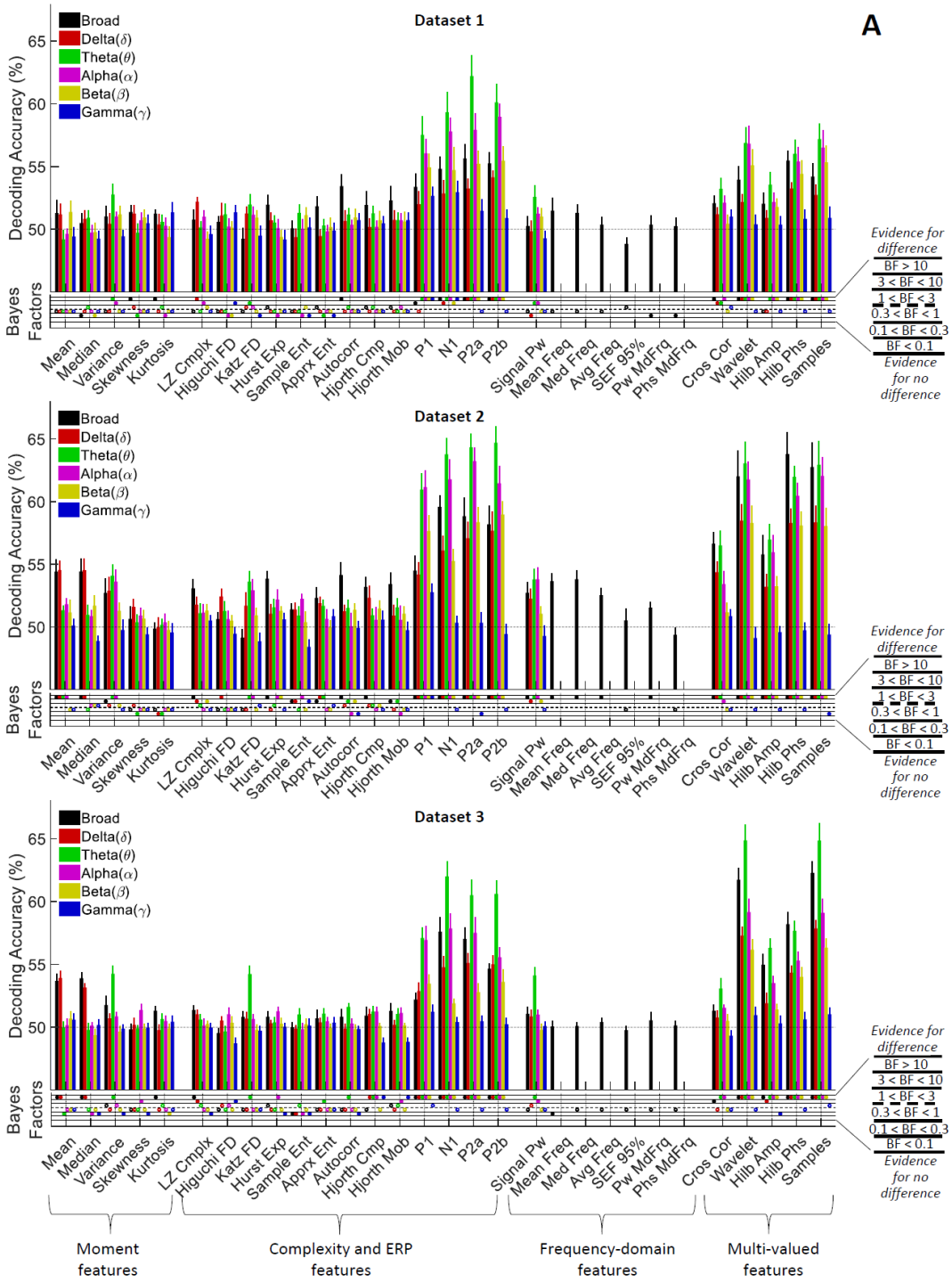

Figure 2. Whole-trial decoding of object categories from the three datasets using 30 features on different frequency bands and Bayesian evidence analyses. (A) Decoding of category information using the 30 features in the 6 frequency bands. The horizontal dashed lines on the top panel refer to chance-level decoding. Thick bars show the average decoding across participants (error bars Standard Error across participants). Bayes Factors are shown in the bottom panel of each graph: Filled circles show moderate/strong evidence for either hypothesis and empty circles indicate insufficient evidence. They show the results of Bayes factor analysis when evaluating the difference from chance-level decoding.

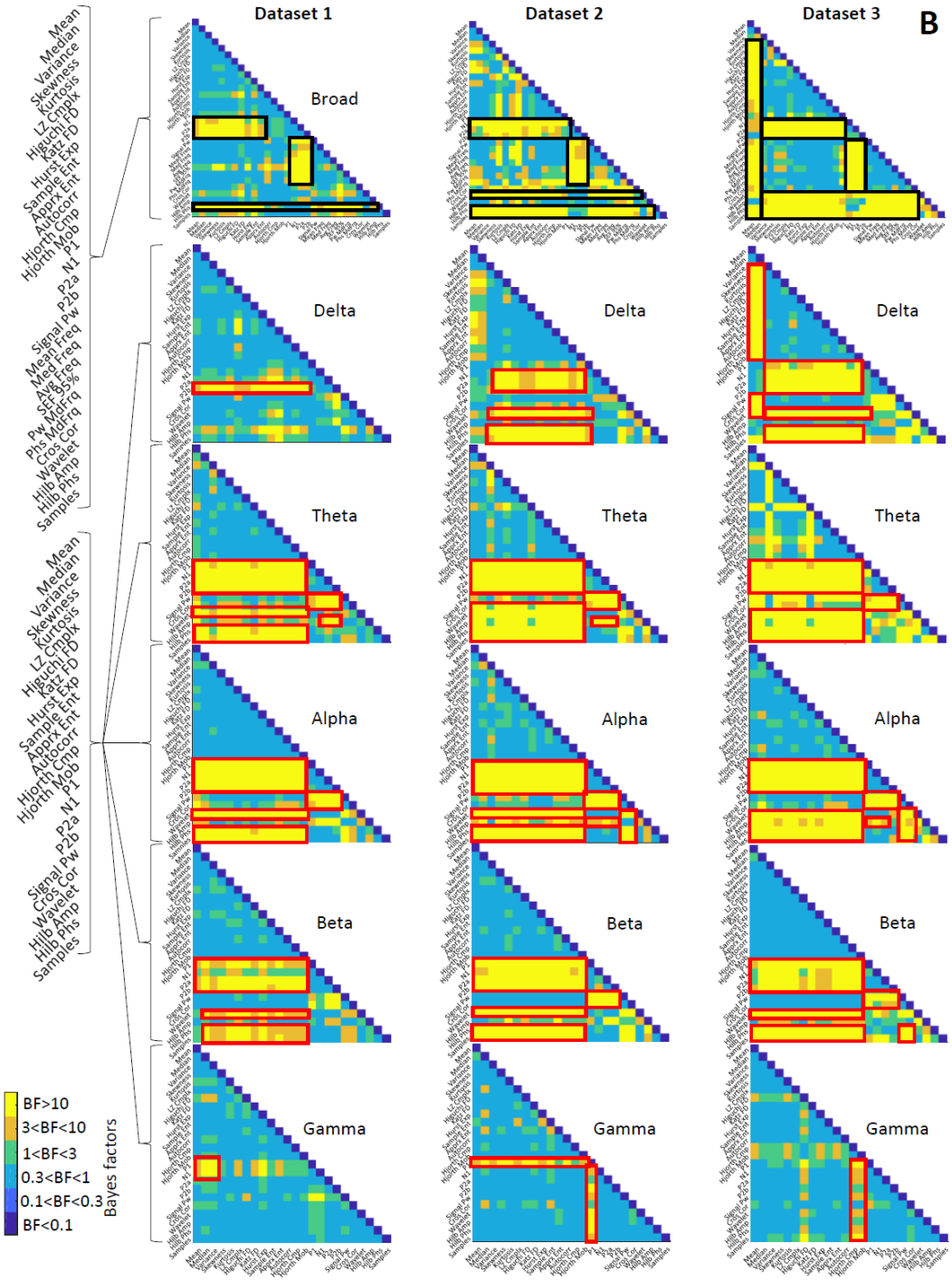

Figure 2. (B) Bayes factor matrices comparing the whole-trial decoding results across different features for each frequency band and dataset separately. Matrices show different levels of evidence for existing difference (moderate 3<BF<10, Orange; strong BF>10, Yellow), no difference (moderate 0.1<BF<0.3, light blue; strong BF<0.1, dark blue) or insufficient evidence (1<BF<3 green; 0.3<BF<1 Cyan) for either hypotheses. Black and red boxes show moderate or strong evidence for higher decoding values for specific features compared other sets of features as explained in the text.

573

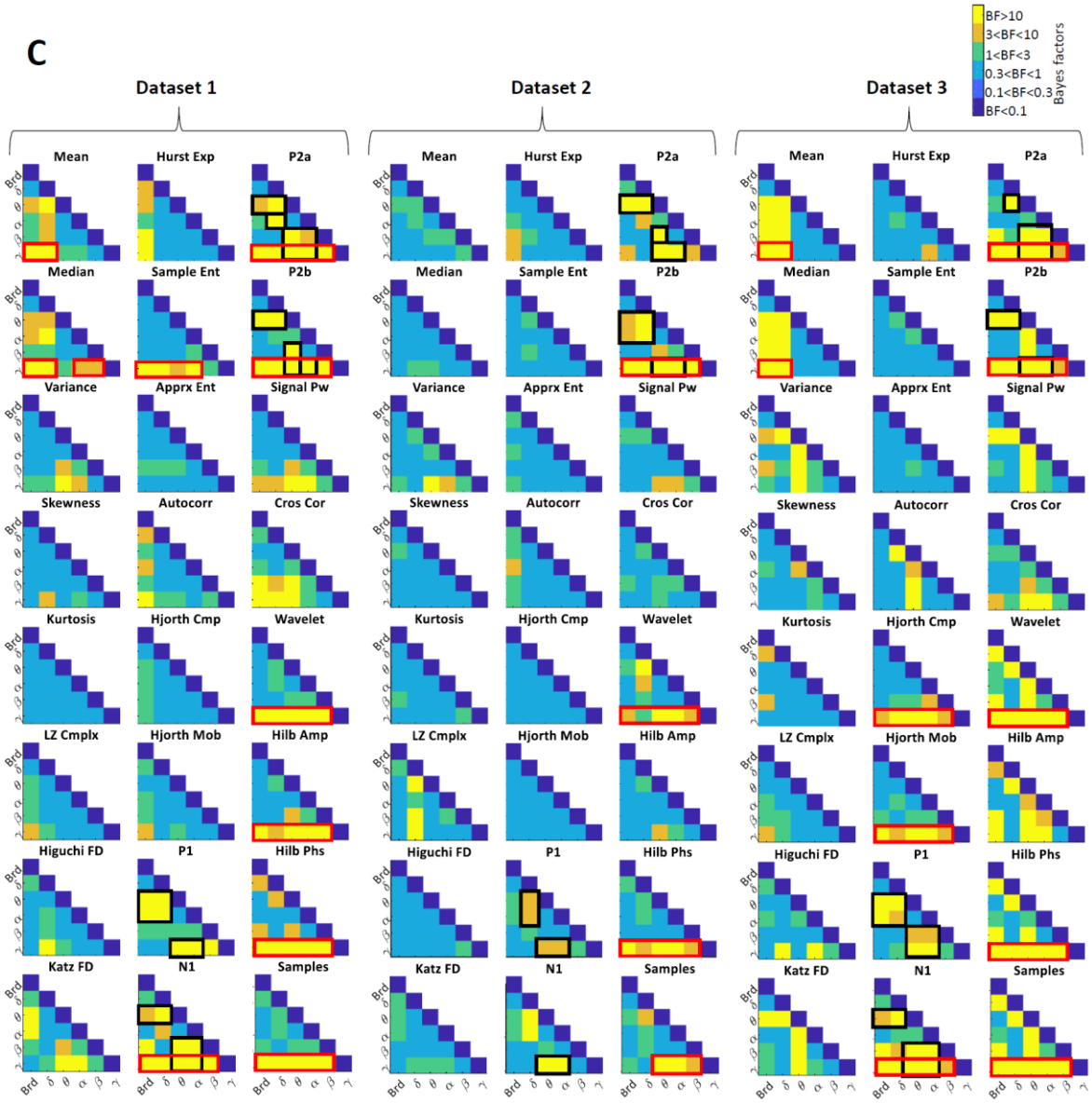

Figure 2. (C) Bayes factor matrices comparing the whole-trial decoding results across different frequency bands for each feature and dataset separately. Matrices show different levels of evidence for existing difference (moderate 3<BF<10, Orange; strong BF>10, Yellow), no difference (moderate 0.1<BF<0.3, light blue; strong BF<0.1, dark blue) or insufficient evidence (1<BF<3 green; 0.3<BF<1 Cyan) for either hypotheses. Black and red boxes show moderate or strong evidence for higher decoding values for specific features compared other sets of features as explained in the text.

Decoding in the Theta band, generally resulted in more features with moderate (3<BF<10) or strong (BF>10) evidence for above-chance decoding, compared to decoding using the broad band signals for datasets 1 and 3 (i.e. 12 and 13 against 13 and 15, respectively). The average theta and alpha band accuracies for all four ERP components surpassed broad-band accuracies in all three datasets (Figure 2A) and N1 and P2b components showed moderate (3<BF<10) or strong (BF>10) evidence to support that in

all datasets (Figure 2C; black boxes). The average of theta band accuracies were also higher than the broad-band accuracies for the Wavelet and Samples in all datasets. There was moderate (3<BF<10) or strong (BF>10) evidence that the gamma band accuracies were lowest among other frequency bands for many features including ERP components and multi-valued features (Figure 2C; red boxes). In datasets 1 and 2, the delta band accuracies were almost as high as the broad-band accuracies for the Mean and Median features, and there was moderate (3<BF<10) or strong (BF>10) evidence that delta band accuracies were higher than other sub-bands in the same datasets. This is consistent with the fact that Mean and Median features capture the average activity, which reflects low-frequency components of the signal time series.

In datasets 1 and 2, where the upper cut-off frequency was 200 Hz rather than 50 Hz in dataset 3, the broad band decoding accuracies were on average higher for majority of complexity features (consisting of Hurst Exp, Apprx Ent, Autocorr, Hjorth Cmp and Mob). The reason might be that the inclusion of more frequency components leads to more informative patterns in the signal, which is captured by the Hurst Exp, Apprx Ent, Autocorr, Hjorth Cmp and Mob, which capture the information from the variability in the data..

Together, frequency band results showed that broad-band signals can provide more information than its sub-bands when using majority of moment or complexity features, which are all from single-valued features. However, ERP components and multi-valued features, which showed the highest information about object categories in the feature set, showed the greatest information in the theta band, even more than which could be achieved using broad-band signals.

What are the temporal dynamics of object category decoding when using distinct features of brain activations?

To answer the second question, we adopted a time-resolved decoding procedure for each feature and dataset separately (see *Methods*). In this method, we repeated the decoding of category information in 50 ms sliding time windows, using a 5 ms step size across the time course of the trials (Figure 3). For a justification of the 50 time window see Supplementary Text 1 and Supplementary Figure 1A. This analysis provided the temporal profile of information encoding as revealed by different features. Note that we do not have the temporal results for time-specific features of ERP components (i.e. P1, N2, P2a and P2b) by definition.

The advantage of the Theta-band to broad-band frequency range, observed for the whole-trial time window (Figure 2A), was also observed for the time-resolved decoding using the Wavelet feature (especially for Dataset 2; with moderate to strong (BF>3) evidence starting to appear after 50 ms post-stimulus onset), but not the Mean feature (Supplementary Figure 1B). However, we used broad-band signals for the time-resolved decoding analyses, because we not only aimed at comparing the information content of the features, but we also aimed at comparing our results with the previous object category decoding studies which used the broad-band frequency range. Note that we do not aim

to maximize the decoding values in this study, but rather aim to compare the decoding results and their correlations to behavior across a wide range of features.

All features in the three datasets showed moderate (3<BF<10) or strong (BF>10) evidence for difference from chance-level decoding at some time points/windows after the stimulus onset. This means that, all features could be used to decode object category information from brain signals. The pairs of decoding curves for the Mean and Median features as well as Wavelet and Samples features were relatively similar/overlapping consistently across the three datasets. Interestingly, however, no pairs of features provided identical patterns of decoding in any of the three datasets as indicated by decoding curves and above-chance Bayes factor analyses. Specifically, while the decoding curves in dataset 1 for several features such as Mean and Median showed two comparable early peaks at around 180 and 300 ms, most other highly informative features (e.g. Variance, Wavelet and Samples) showed only one peak at around 180 ms. There was only one dominant peak for Mean, Median and frequency-domain and multi-valued features in datasets 2 and 3 and two dominant peaks for the other features including the complexity and moment features. This discrepancy can be explained by many parameters which differ across the three datasets, including the stimuli, task, presentation paradigm, etc.

Consistently across the three datasets, for all features, there was moderate (3<BF<10) or strong (BF>10) evidence for above-chance decoding starting to appear from around 80 ms. The decoding curves returned back to the chance-level around than 500 ms, particularly for the most informative features such as Mean, Median and multi-valued features in dataset 1. The same features remained above chance (BF>3) up until 550 ms (dataset 2) or even later than 800 ms (dataset 3). This difference can be potentially because of the longer stimulus presentation time for datasets 2 and 3, which provided stronger sensory input for processing of category information (Grootswagers et al., 2019).

We calculated several time and amplitude-related parameters from the decoding curves for a quantitative comparison between the decoding patterns of different features. These parameters consist of maximum and average decoding accuracies, the time to the first above-chance and maximum decoding. The parameters were extracted from decoding curves in the post-stimulus window (0 to 1000 ms; Figure 4), and have provided important implications for studying the dynamics of object recognition in the human brain (Isik et al., 2014).

Consistently across the three datasets, there was strong evidence that all features from all three datasets had above-chance maximum decoding accuracy (Figure 4A; colored dots in the bottom Bayes Factors' panels). The features of Mean, Median, Wavelet and Samples obtained the highest maximum and average decoding accuracies among other features (Figure 4A; black boxes). There was strong (BF>10) evidence that Wavelet had the highest maximum decoding accuracy compared to all other features (except Samples in all three datasets and Mean and Median in dataset 2).

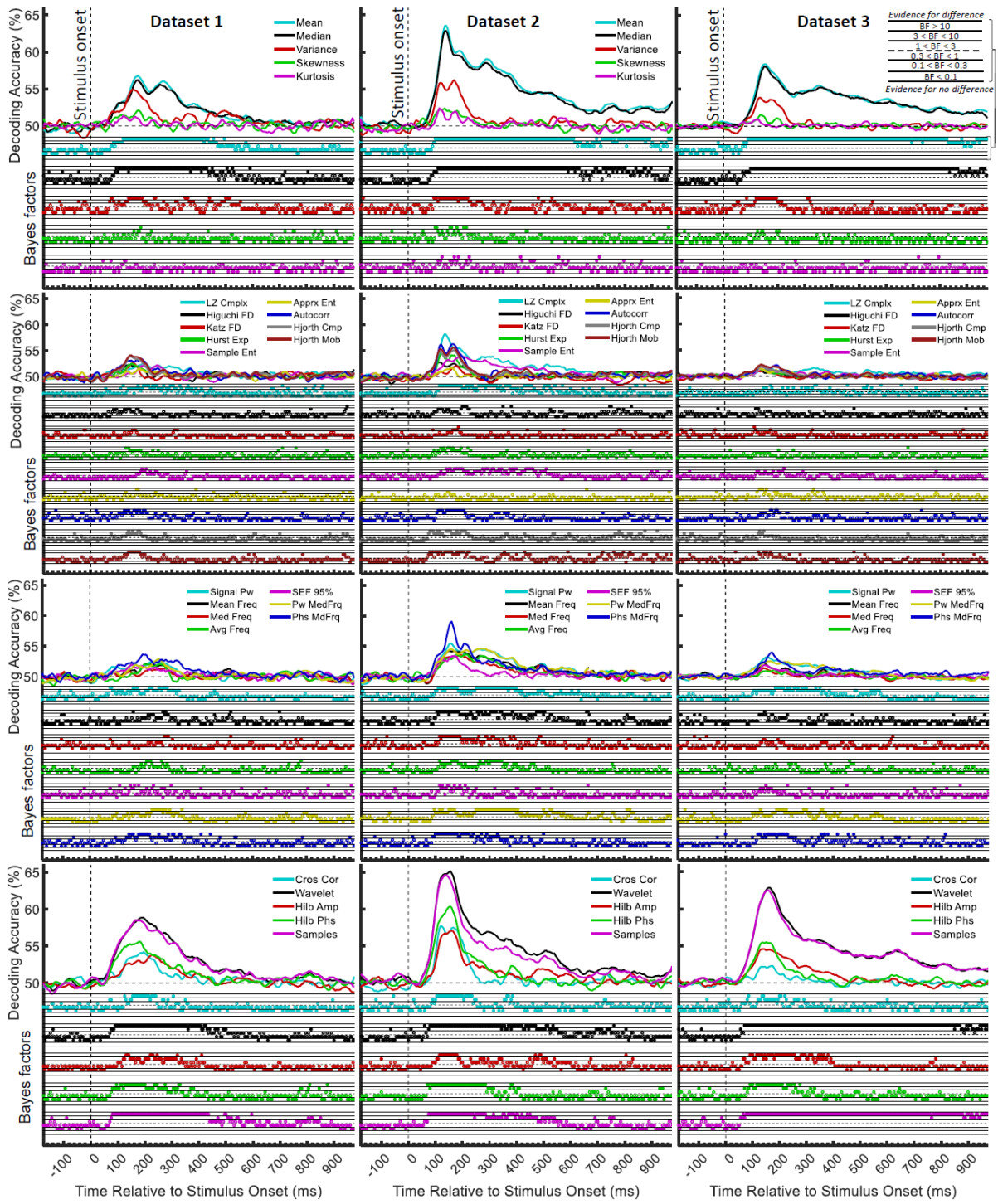

Figure 3. Time-resolved decoding of object categories from the three datasets using 26 features and Bayesian evidence analyses. Each row shows the results of one type of feature (i.e. moment, complexity, frequency-domain and multi-valued features from top to bottom, respectively). Each column shows the results for one dataset. Top section in each panel shows the decoding accuracies across time and the bottom section shows the Bayes factor evidence for the difference of the decoding accuracy compared to chance-level decoding. The horizontal dashed lines on the top panel refer to chance-level decoding. Filled circles in the Bayes Factors show moderate/strong evidence for either difference or no difference from chance-level decoding and empty circles indicate insufficient evidence for either hypotheses.

Although there was strong (BF>10) evidence that Mean, Median, Wavelet and Samples provided above-chance average accuracy across the three datasets, there was insufficient (0.3<BF<1) evidence for above-chance average accuracy for several other features (e.g. Katz FD). The patterns of average decoding accuracies correlated with the pattern of maximum decoding accuracies across features ($r > 0.9$; $p < 0.01$; Supplementary Text 2 and Supplementary Figure 2A) with Mean, Median, Wavelet and Samples dominating other features (Figure 4B; black boxes). Although no quantitative comparison was made across the datasets, as they are incomparable because of so many different variables, dataset 2, seems to provide the highest amount of category information, for the reason of which was explained above. Interestingly, Katz FD, which has been previously shown to be very informative in category decoding (Torabi et al., 2017), is among the least (if not the least) informative feature.

The time to maximum decoding was interesting in that, many of the features showed a maximum time in the range of 150 to 220 ms, and there was no clear trend towards any feature types (Figure 4C). There was moderate (3<BF<10) evidence that Median reached its maximum decoding after moment features of Variance, Skewness and Kurtosis in dataset 1. There was moderate (3<BF<10) or strong (BF>10) that Katz FD was among the fastest features to reach its maximum decoding in dataset 1. There was moderate (3<BF<10) or strong (BF>10) evidence that Wavelet, Hilb Phs and Samples were among the fastest features to reach their maximum values in datasets 2 and 3.

The time of first above-chance (BF>3) decoding did not show the domination of any specific set of features relative to others (i.e. significantly faster or slower features; Figure 4D). There was moderate (3<BF<10) or strong (BF>10) evidence that Mean, Median, Wavelet and Samples showed an earlier time to above-chance decoding compared to Sample Ent, Avg Freq, Med Freq, SEF 95%, Cros Cor and Katz FD in dataset 1. There was moderate (3<BF<10) evidence that Hjorth Cmp and Mob, were among the earliest features to show decoding on dataset 2. The time of first above-chance and maximum decoding correlated in datasets 2 and 3 but not dataset 1 ($r=0.67$, $r=0.51$ and $r=0.02$ respectively for datasets 1, 2 and 3; Supplementary Text 2 and Supplementary Figure 2A). The correlation analyses between amplitude and timing parameters showed that features which provided a higher maximum decoding also showed a higher average decoding and vice versa. On the other hand, features that reached their above-chance decoding earlier also reached their maximum decoding earlier. This suggests that, more informative features, such as Wavelet, not only provided the most information about object categories, but they also captured the earliest evidence of category-related information from brain activity.

In conclusion, the features of Mean, Median, Wavelet and Samples (i.e. which refers to the samples of the signal), not only provided the maximum and average amount of category-related information in the brain, but they also were among the earliest features that provided signatures of object category information in the brain at around 100 ms. These results also suggest that object category information peaked at around 180 ms after the stimulus onset, irrespective of the feature used for decoding of information.

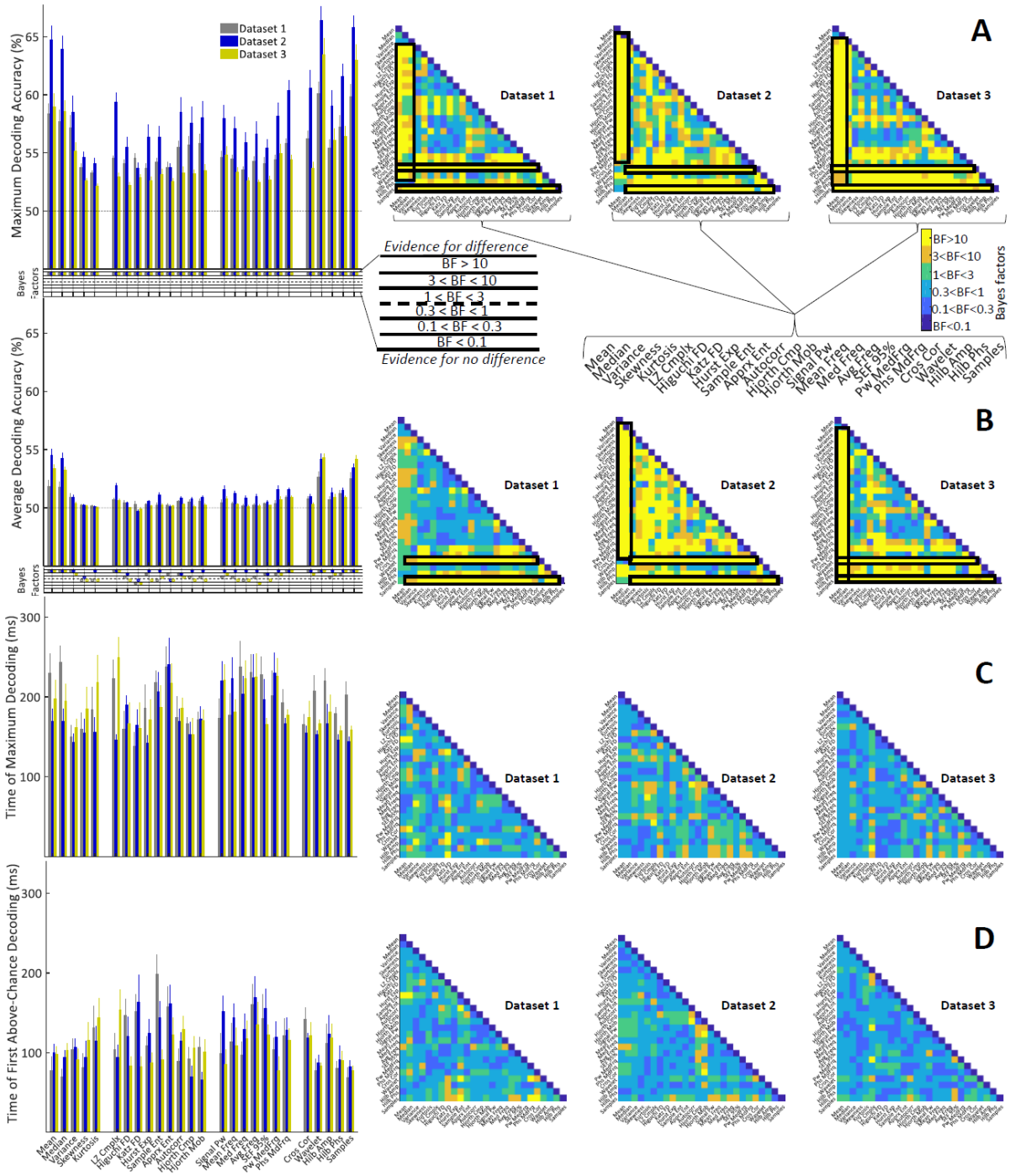

Figure 4. Timing and amplitude parameters extracted from the time-resolved accuracies of each feature and each dataset and their Bayesian evidence analyses. (A-D) Left: the maximum and average decoding accuracies, the time of maximum and the first above-chance decoding. Bottom section on A and B show the Bayes factor evidence for the difference of the decoding accuracy compared to chance-level decoding; Right: matrices compare the right parameters obtained from different features. Different levels of evidence for existing difference (moderate 3<BF<10, Orange; strong BF>10, Yellow), no difference (moderate 0.1<BF<0.3, light blue; strong BF<0.1, dark blue) or insufficient evidence (1<BF<3 green; 0.3<BF<1 Cyan) for either hypotheses. Black and red boxes show moderate or strong evidence for higher decoding values for specific features compared other sets of features as explained in the text. The horizontal dashed lines on the left panels of (A) and (B) refer to chance-level decoding. Filled circles in the Bayes Factors show moderate/strong evidence for either hypothesis and empty circles indicate insufficient evidence.

Which features of brain activations explain behavioral recognition performance?

To answer the third question of this study, we calculated the *correlation* between the decoding accuracies obtained from each feature and the reaction times of participants at every time point around the stimulus onset (Karimi-Rouzbahani et al., 2019; Karimi-Rouzbahani et al., 2020a). Participants' reaction time in object recognition has been previously shown to be predictable from decoding accuracy (Ritchie et al., 2015). We expected to observe negative correlation values between decoding accuracies and participants' reaction time in the post-stimulus span, meaning that greater separability across neural representations of object categories would lead to/correlate with faster recognition of the corresponding categories. For this analysis, we only used dataset 2 as it was the only dataset with an active object detection task; therefore recording recognition reaction times. To calculate the correlations, we generated a 10-dimensional vector of neural decoding accuracies at every time point and a 10-dimensional vector for behavioral reaction times obtained from the group of 10 participants and correlated the two vectors across the time course of trials using Spearman's rank correlation. This resulted in a single correlation value for each time point for the whole group of participants.

All features, except Katz FD, showed negative trends after the stimulus onset (Figure 5A). No two features showed identical time courses for correlations. The negative correlations did not remain significant for long spans of the time, except for multi-valued features, which showed more pronounced negative correlations that remained significant for larger spans of time. Correlations also showed larger negative peaks (generally < -0.5) for multi-valued features especially Wavelet, compared to other features (generally > -0.5). Specifically, while higher-order moment features (i.e. Variance, Skewness and Kurtosis) as well as many complexity features showed earlier peaks of negative correlations at around 150 ms, Mean, Median, frequency-domain features and multi-valued features showed later negative peaks after 300 ms. The multi-valued features (especially Wavelet), Mean, Median, which dominated other features in terms of decoding accuracy (Figures 2-4), showed also the largest window of negative correlations to behavior.

Together, it seems that features with the highest decoding accuracy were also better at explaining behavioral performance. This was reflected in their longer time windows and larger negative peaks of their correlations to behavioral reaction time. To quantitatively assess this hypothesis, we calculated the correlation between different parameters of the decoding accuracy curves (Figure 4; consisting of average and maximum decoding accuracy, the time to the first above-chance and maximum decoding) and the average correlation-to-behavior obtained for the same features (obtained from Figure 5A). To obtain the average correlation-to-behavior, we simply averaged the 'correlation to behavior' in the post-stimulus time span. Results showed that (Figure 5B), while the temporal parameters of 'time of first above-chance' and 'maximum' decoding failed to predict the level of correlation to behavior ($r=0.27$, $p=0.27$, and $r=0.18$, $p=0.37$, respectively), the amplitude parameters of 'maximum' and 'average' decoding accuracies of features significantly ($r=-0.71$ and $r=-0.72$ respectively, with $p<0.0001$; Pearson's correlation) predicted the average correlation between the features' decoding accuracies and prediction power of the parameter.

739

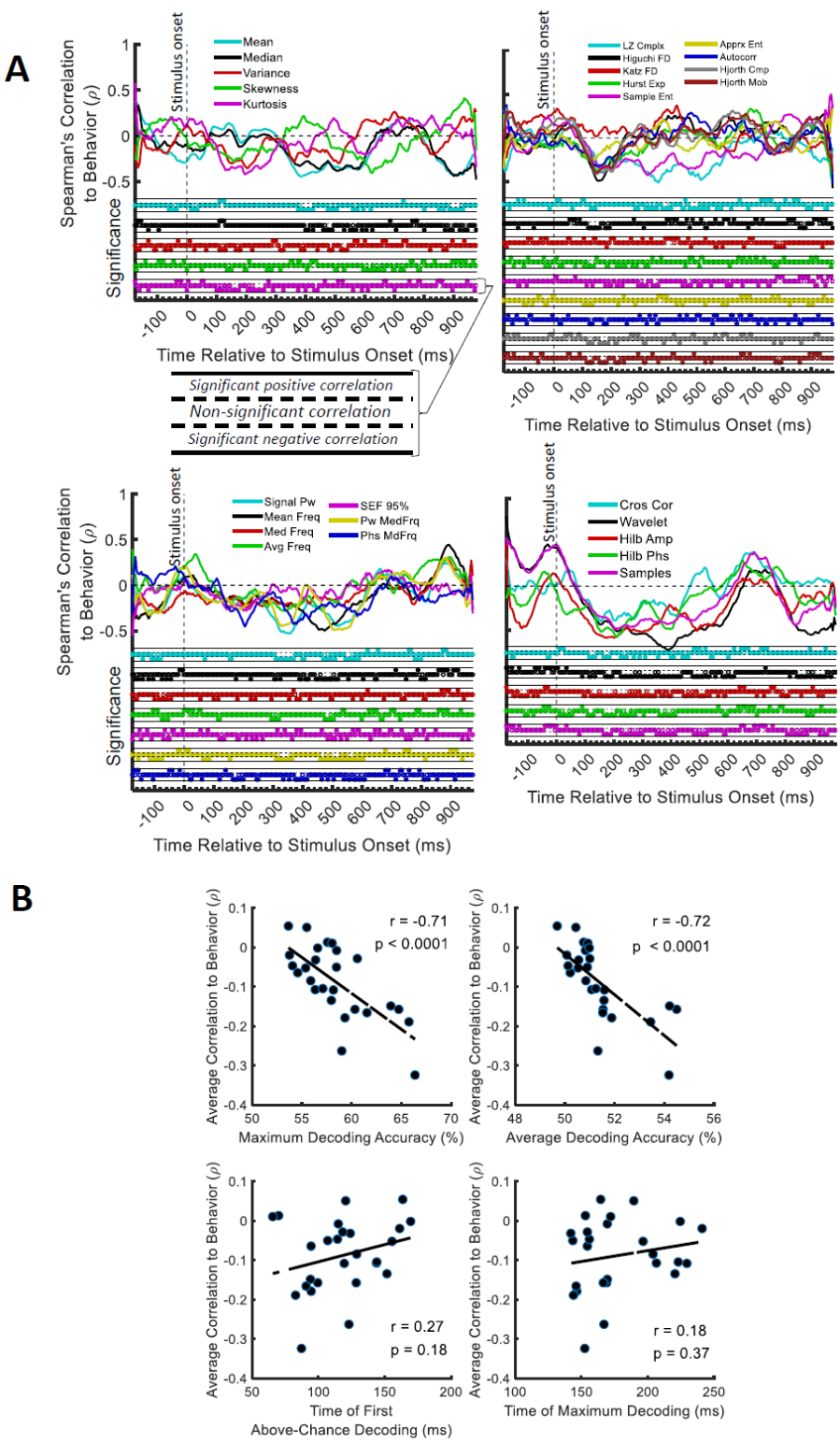

Figure 5. Correlation between the decoding accuracies and behavioral reaction time. (A) Top section in each panel shows the (Spearman's) correlation coefficient obtained from correlating the decoding values and the reaction times for each feature separately. Bottom section shows positively or negatively significant (P<0.05; filled circles) or non-significant (p>0.05; empty circles) correlations as evaluated by random permutation of the variables in correlation. (B) Correlation between each of the amplitude and timing parameters of time-resolved decoding (i.e. maximum and average decoding accuracy and time of first and maximum decoding) with the average time-resolved correlations calculated from (A) for the set of N=26 features. The slant line shows the best linear fit to the distribution of the correlation data.

This result suggests that features that provided more information about object categories (i.e. decoded object categories with higher accuracy), predicted behavioral performance better. This may suggest that, better extraction of category-related information from brain activations, which has been achieved through the choice of features such as Wavelet, can lead to more accurate prediction of behavioral performance in object recognition. This is not a trivial result, which might incorrectly be expected to be caused by a higher decoding value for the more informative features leading to a higher correlation to behavior. This is because, the mathematical calculation of the 'correlation coefficient' standardizes the variables, so that the changes in scale/amplitude will not affect its value.

Discussion

This study compared a large set of statistical and mathematical features (30, the largest to date) from EEG signals for their object category-related information using neural decoding in different frequency bands. Results showed that, the Theta frequency band provided more information about object categories than the conventionally used broad-band activity, whether analyzing the whole trial or temporally resolving the decoding. We showed that multi-valued features such as signal Samples and Wavelet coefficients can provide information up and above the conventional feature of Mean brain activity, which overlooks the temporal variations in the time series. We also showed that the Wavelet feature, not only provided the highest decoding accuracy, but it also explained the behavioral object recognition performance better than all the other features. As the mentioned results were consistent across three datasets, which had been collected across a wide range of variations, the generalizability of the results are far more than the previous studies. Our results suggest that improving the performance in decoding could be a path for improving the behavioral explanatory power in neural data analysis, which can help filling the gap between neuroimaging and behavior.

This study provides new insights for the fields of cognitive neuroscience and BCI at the same time. In the past two decades, many neuroimaging studies in cognitive neuroscience have tried to provide insights into the spatiotemporal dynamics of object category processing in the human brain (Haxby et al., 2001; Contini et al., 2017; Carlson et al., 2013). This study does not provide any information about the spatial location of object category information processing in the brain. From the temporal viewpoint, however, it suggests that to access more variance in the neural code, we need to take the temporal variability of the neural activations into account when running multivariate pattern analyses. This aligns with the recent shift towards taking into account the temporal variability of trials when decoding visual information from high-temporal resolution methods such as MEG (Vidaurre et al., 2019). Importantly, our results showed that, multi-valued features such as original signal Samples and Wavelet coefficients, could provide information up and above which could be achieved using the conventional Mean-based decoding analyses (Grootswagers et al., 2017). This is because, with (i.e. Wavelet) or without any transformation (i.e. Samples), these features extracted the most informative sample/data window within the sliding time window. This supports previous studies which show that the temporal patterns of activity could provide information regarding the co-occurrences of visual edges (Eckhorn et al., 1988) and orientation in primary visual cortex (Celebrini et al., 1993) as well as light intensity in the retina (Gollisch and Meister, 2008). This is also consistent with more recent findings in object recognition

781 suggesting a role for the temporal phase (Behroozi et al., 2015) or within-trial correlation in the
782 temporal cortex (Majima et al., 2014). However, none of the mentioned studies have validated their
783 results across multiple datasets to provide a more generalizable view on object category encoding in the
784 human brain. Moreover, the advantage of the Theta band, to all the other frequency bands evaluated in
785 this study, is consistent with the observation of Theta band being involved in the processing of feed-
786 forward visual information (Bastos et al., 2015), which is dominant in the evaluated object recognition
787 paradigms, where participants' tasks were minimal.

788

789 Another important question in cognitive neuroscience has been whether (if at all) neuroimaging data
790 can explain behavior (Williams et al., 2007; Ritchie et al., 2015; Woolgar et al., 2019). Although many
791 recent studies have found correlations between the neural decoding and behavioral performance in
792 object and face recognition (Karimi-Rouzbahani et al., 2019; Karimi-Rouzbahani et al., 2020a; Dobs et al.,
793 2019), as we also did in the current study, one question that has remained unanswered was whether a
794 more optimal neural code for objects, which is found using feature extraction, could explain the
795 behavioral performance more accurately. This study, for the first time, compared the explanatory power
796 of a large set of signal features and found that, the features which provided more information about
797 object categories, also explained the behavioral performance more accurately than those which
798 provided less information.

799

800 As for the field of visual-representation-based BCI, in which the aim is to improve the decoding
801 performance for improved brain-computer interaction (Wang et al., 2012; Van Gerven et al., 2009), this
802 study provides new suggestions. Specifically, we showed that, when considering the whole-trail data,
803 which is usually the case in BCI, the ERP components and the multi-valued features provided the highest
804 amount of information about object categories, and it is most pronounced in the Theta band. None of
805 the previous studies, which used the ERP components (Wang et al., 2012; Qin et al., 2016; Jadidi et al.,
806 2016) or the Wavelet transformation (Taghizadeh-Sarabi et al., 2015; Torabi et al., 2017), limited their
807 frequency band to the Theta band, which here showed higher decoding accuracy in both the whole-trial
808 ERP components (Figure 2) as well as sliding-window Wavelet component (Supplementary Figure 1B).
809 Therefore, the next step in visual-representation-based BCI might be looking at specific frequency sub-
810 bands.

811

812 While many studies have used supervised computational algorithms such as Common Spatial Patterns
813 (Murphy et al., 2011), Voltage Topographies (Tzovara et al., 2011), Independent Component Analysis
814 (Stewart et al., 2014) and Convolutional Neural Networks (Seeliger et al., 2017), the focus of the current
815 study was to compare the inherent codes already available in brain representations through statistical
816 and computational feature extraction. In other words, we made no adjustments to these features to
817 provide category-separable representations and extracted them directly from the time series data. This
818 is because, rather than trying to maximize the separability/decodeability of representations across
819 object categories, we mainly aimed at gaining insight into how the brain encodes this information by
820 determining which of the available statistical features could capture/crack these codes. Accordingly,
821 there might be many supervised algorithms, particularly in the area of BCI, which can provide higher

decoding accuracies than those obtained from individual features of this study. Moreover, if we had not reduced the dimensionality of the data for the multi-valued features for the sake of comparison with single-valued features, the decoding performance would likely increase as it has been the case in previous studies (Taghizadeh-Sarabi et al., 2015; Torabi et al., 2017).

There are several future directions for this research. One main question is how the results of this study generalize to other cognitive processes such as attention, memory, decision making, etc. In other words, it is interesting to know what the most informative features would be when decoding different conditions in a memory or attention task. Another interesting observation that we had in the current study was that shorter time windows of signals (i.e. 5 ms) tended to provide larger initial (0 ms<t<200 ms) peaks in decoding compared to longer ones (i.e. 100 ms), while the latter provided higher decoding values in later stages of the trial (t > 200; Supplementary Figure 1A). This was more pronounced for dataset 2, which had an active task and a longer presentation time. It suggests that, it could be the case that initial stages of object category processing (e.g. extraction of visual features) takes a shorter time spans, while later stages (e.g. association of visual information to categories or recurrence/feedback processing) take longer time spans. Therefore, we might need a time-variable sliding window for different stages of object recognition or any other cognitive processes to truly capture the temporal dynamics of cognition. Another interesting extension to this work can be studying how (if at all) a combination of the features used in this study could provide added information about object categories and/or behavior. In other words, although all of the individual features evaluated here covered some variance of category object information, to obtain the full variance of the actual neural code, we might need to combine multiple features. To that end, we can combine the extracted features using a variety of supervised and un-supervised methods as have previously provided additional information (Karimi Rouzbahani et al., 2011; Qin et al., 2016).

The cross-dataset, large-scale analysis methods implemented in this study aligns with the growing trend towards meta-analyses in cognitive neuroscience. Recent studies have also adopted and compared several datasets to facilitate forming more rigorous conclusions about how the brain performs different cognitive processes such as sustained attention (Langner et al., 2013) or working memory (Adam et al., 2020). Our exploratory analysis presented here, has also the advantage that it was not biased towards any of the findings. We simply compared sets of features from the EEG signals to see which one provides more information about object categories and which one best explain behavior. The findings of this study provide generalizable insights into the most informative features of EEG signals in object category processing.

References

Adam, K.C., Vogel, E.K. and Awh, E., 2020. Multivariate analysis reveals a generalizable human electrophysiological signature of working memory load. *bioRxiv*.

Bastos, A.M., Vezoli, J., Bosman, C.A., Schoffelen, J.M., Oostenveld, R., Dowdall, J.R., De Weerd, P., Kennedy, H. and Fries, P., 2015. Visual areas exert feedforward and feedback influences through distinct frequency channels. *Neuron*, *85*(2), pp.390-401.

Behroozi, M., Daliri, M.R. and Shekarchi, B., 2016. EEG phase patterns reflect the representation of semantic categories of objects. *Medical & biological engineering & computing*, *54*(1), pp.205-221.

Carlson, T., Tovar, D.A., Alink, A. and Kriegeskorte, N., 2013. Representational dynamics of object vision: the first 1000 ms. *Journal of vision*, *13*(10), pp.1-1.

Celebrini, S., Thorpe, S., Trotter, Y. and Imbert, M., 1993. Dynamics of orientation coding in area V1 of the awake primate. *Visual neuroscience*, *10*(5), pp.811-825.

Chan, A.M., Halgren, E., Marinkovic, K. and Cash, S.S., 2011. Decoding word and category-specific spatiotemporal representations from MEG and EEG. *Neuroimage*, *54*(4), pp.3028-3039.

Cichy, R.M., Pantazis, D. and Oliva, A., 2014. Resolving human object recognition in space and time. *Nature neuroscience*, *17*(3), p.455.

Contini, E.W., Wardle, S.G. and Carlson, T.A., 2017. Decoding the time-course of object recognition in the human brain: From visual features to categorical decisions. *Neuropsychologia*, *105*, pp.165-176.

Dienes, Z., 2014. Using Bayes to get the most out of non-significant results. *Frontiers in psychology*, *5*, p.781.

Dobs, K., Isik, L., Pantazis, D. and Kanwisher, N., 2019. How face perception unfolds over time. *Nature communications*, *10*(1), pp.1-10.

Eckhorn, R., Bauer, R., Jordan, W., Brosch, M., Kruse, W., Munk, M. and Reitboeck, H.J., 1988. Coherent oscillations: A mechanism of feature linking in the visual cortex?. *Biological cybernetics*, *60*(2), pp.121-130.

Gollisch, T. and Meister, M., 2008. Rapid neural coding in the retina with relative spike latencies. *Science*, *319*(5866), pp.1108-1111.

Grootswagers, T., Cichy, R.M. and Carlson, T.A., 2018. Finding decodable information that can be read out in behaviour. *NeuroImage*, *179*, pp.252-262.

Grootswagers, T., Robinson, A.K. and Carlson, T.A., 2019. The representational dynamics of visual objects in rapid serial visual processing streams. *NeuroImage*, *188*, pp.668-679.

Grootswagers, T., Wardle, S.G. and Carlson, T.A., 2017. Decoding dynamic brain patterns from evoked responses: A tutorial on multivariate pattern analysis applied to time series neuroimaging data. Journal of cognitive neuroscience, 29(4), pp.677-697.

Guo, L., Rivero, D., Seoane, J.A. and Pazos, A., 2009. Classification of EEG signals using relative wavelet energy and artificial neural networks. In *Proceedings of the first ACM/SIGEVO Summit on Genetic and Evolutionary Computation* (pp. 177-184).

Hatamimajoumerd, E. and Talebpour, A., 2019. A Temporal neural trace of wavelet coefficients in human object vision: an MEG study. *Frontiers in neural circuits*, *13*, p.20.

Hatamimajoumerd, E., Talebpour, A. and Mohsenzadeh, Y., 2019. Enhancing multivariate pattern analysis for magnetoencephalography through relevant sensor selection. *International Journal of Imaging Systems and Technology*.

Haxby, J.V., Gobbini, M.I., Furey, M.L., Ishai, A., Schouten, J.L. and Pietrini, P., 2001. Distributed and overlapping representations of faces and objects in ventral temporal cortex. *Science*, *293*(5539), pp.2425-2430.

Higuchi, T., 1988. Approach to an irregular time series on the basis of the fractal theory. *Physica D: Nonlinear Phenomena*, *31*(2), pp.277-283.

Hjorth, B., 1970. EEG analysis based on time domain properties. *Electroencephalography and clinical neurophysiology*, *29*(3), pp.306-310.

Hung, C.P., Kreiman, G., Poggio, T. and DiCarlo, J.J., 2005. Fast readout of object identity from macaque inferior temporal cortex. Science, 310(5749), pp.863-866.

Iranmanesh, S. and Rodriguez-Villegas, E., 2017. An Ultralow-Power Sleep Spindle Detection System on Chip. *IEEE transactions on biomedical circuits and systems*, *11*(4), pp.858-866.

Isik, L., Meyers, E.M., Leibo, J.Z. and Poggio, T., 2014. The dynamics of invariant object recognition in the human visual system. *Journal of neurophysiology*, *111*(1), pp.91-102.

Jadidi, A.F., Zargar, B.S. and Moradi, M.H., 2016, November. Categorizing visual objects; using ERP components. In *2016 23rd Iranian Conference on Biomedical Engineering and 2016 1st International Iranian Conference on Biomedical Engineering (ICBME)* (pp. 159-164). IEEE.

Jeffreys, H., 1998. *The theory of probability*. OUP Oxford.

Joshi, D., Panigrahi, B.K., Anand, S. and Santhosh, J., 2018. Classification of Targets and Distractors Present in Visual Hemifields Using Time-Frequency Domain EEG Features. *Journal of healthcare engineering*, *2018*.

Kaneshiro, B., Guimaraes, M.P., Kim, H.S., Norcia, A.M. and Suppes, P., 2015. A representational similarity analysis of the dynamics of object processing using single-trial EEG classification. *Plos one*, *10*(8).

Karimi Rouzbahani, H. and Daliri, M.R., 2011. Diagnosis of Parkinson's disease in human using voice signals. *Basic and Clinical Neuroscience*, *2*(3), pp.12-20.

Karimi-Rouzbahani, H., 2018. Three-stage processing of category and variation information by entangled interactive mechanisms of peri-occipital and peri-frontal cortices. *Scientific reports*, *8*(1), pp.1-22.

Karimi-Rouzbahani, H., Bagheri, N. and Ebrahimpour, R., 2017a. Average activity, but not variability, is the dominant factor in the representation of object categories in the brain. *Neuroscience*, *346*, pp.14-28.

Karimi-Rouzbahani, H., Bagheri, N. and Ebrahimpour, R., 2017b. Hard-wired feed-forward visual mechanisms of the brain compensate for affine variations in object recognition. *Neuroscience*, *349*, pp.48-63.

Karimi-Rouzbahani, H., Bagheri, N. and Ebrahimpour, R., 2017c. Invariant object recognition is a personalized selection of invariant features in humans, not simply explained by hierarchical feed-forward vision models. Scientific reports, 7(1), pp.1-24.

Karimi-Rouzbahani, H., Ramezani, F., Woolgar, A., Rich, A.N., Ghodrati, M., 2020a. Perceptual difficulty modulates the direction of information flow in familiar face recognition.

Karimi-Rouzbahani, H., Vahab, E., Ebrahimpour, R. and Menhaj, M.B., 2019. Spatiotemporal analysis of category and target-related information processing in the brain during object detection. *Behavioural brain research*, *362*, pp.224-239.

Karimi-Rouzbahani, H., Woolgar, A. and Rich, A.N., 2020b. Neural signatures of vigilance decrements predict behavioural errors before they occur. *bioRxiv*.

Katz, M.J., 1988. Fractals and the analysis of waveforms. *Computers in biology and medicine*, *18*(3), pp.145-156.

Kiani, R., Esteky, H., Mirpour, K. and Tanaka, K., 2007. Object category structure in response patterns of neuronal population in monkey inferior temporal cortex. *Journal of neurophysiology*, *97*(6), pp.4296-4309.

Kriegeskorte, N., Mur, M., Ruff, D.A., Kiani, R., Bodurka, J., Esteky, H., Tanaka, K. and Bandettini, P.A., 2008. Matching categorical object representations in inferior temporal cortex of man and monkey. *Neuron*, *60*(6), pp.1126-1141.

Langner, R. and Eickhoff, S.B., 2013. Sustaining attention to simple tasks: a meta-analytic review of the neural mechanisms of vigilant attention. *Psychological bulletin*, *139*(4), p.870.

Lee, M.D. and Wagenmakers, E.J., 2005. Bayesian statistical inference in psychology: Comment on Trafimow (2003).

Lempel, A. and Ziv, J., 1976. On the complexity of finite sequences. *IEEE Transactions on information theory*, *22*(1), pp.75-81.

Liu, H., Agam, Y., Madsen, J.R. and Kreiman, G., 2009. Timing, timing, timing: fast decoding of object information from intracranial field potentials in human visual cortex. *Neuron*, *62*(2), pp.281-290.

Majima, K., Matsuo, T., Kawasaki, K., Kawai, K., Saito, N., Hasegawa, I. and Kamitani, Y., 2014. Decoding visual object categories from temporal correlations of ECoG signals. *Neuroimage*, *90*, pp.74-83.

Miyakawa, N., Majima, K., Sawahata, H., Kawasaki, K., Matsuo, T., Kotake, N., Suzuki, T., Kamitani, Y. and Hasegawa, I., 2018. Heterogeneous Redistribution of Facial Subcategory Information Within and Outside the Face-Selective Domain in Primate Inferior Temporal Cortex. *Cerebral Cortex*, *28*(4), pp.1416-1431.

Murphy, B., Poesio, M., Bovolo, F., Bruzzone, L., Dalponte, M. and Lakany, H., 2011. EEG decoding of semantic category reveals distributed representations for single concepts. *Brain and language*, *117*(1), pp.12-22.

Norman, K.A., Polyn, S.M., Detre, G.J. and Haxby, J.V., 2006. Beyond mind-reading: multi-voxel pattern analysis of fMRI data. *Trends in cognitive sciences*, *10*(9), pp.424-430.

Pincus, S.M. and Huang, W.M., 1992. Approximate entropy: statistical properties and applications. *Communications in Statistics-Theory and Methods*, *21*(11), pp.3061-3077.

Pulini, A.A., Kerr, W.T., Loo, S.K. and Lenartowicz, A., 2019. Classification accuracy of neuroimaging biomarkers in attention-deficit/hyperactivity disorder: Effects of sample size and circular analysis. Biological Psychiatry: Cognitive Neuroscience and Neuroimaging, 4(2), pp.108-120.

Qin, Y., Zhan, Y., Wang, C., Zhang, J., Yao, L., Guo, X., Wu, X. and Hu, B., 2016. Classifying four-category visual objects using multiple ERP components in single-trial ERP. *Cognitive neurodynamics*, *10*(4), pp.275-285.

Racine, R., 2011. Estimating the Hurst exponent. *Zurich: Mosaic Group*.

Richman, J.S. and Moorman, J.R., 2000. Physiological time-series analysis using approximate entropy and sample entropy. *American Journal of Physiology-Heart and Circulatory Physiology*, *278*(6), pp.H2039-H2049.

Ritchie, J.B., Tovar, D.A. and Carlson, T.A., 2015. Emerging object representations in the visual system predict reaction times for categorization. *PLoS computational biology*, *11*(6).

Rouder, J.N., Morey, R.D., Speckman, P.L. and Province, J.M., 2012. Default Bayes factors for ANOVA designs. *Journal of Mathematical Psychology*, *56*(5), pp.356-374.

Rupp, K., Roos, M., Milsap, G., Caceres, C., Ratto, C., Chevillet, M., Crone, N.E. and Wolmetz, M., 2017. Semantic attributes are encoded in human electrocorticographic signals during visual object recognition. *NeuroImage*, *148*, pp.318-329.

Seeliger, K., Fritsche, M., Güçlü, U., Schoenmakers, S., Schoffelen, J.M., Bosch, S.E. and Van Gerven, M.A.J., 2018. Convolutional neural network-based encoding and decoding of visual object recognition in space and time. *NeuroImage*, *180*, pp.253-266.

Simanova, I., Van Gerven, M., Oostenveld, R. and Hagoort, P., 2010. Identifying object categories from event-related EEG: toward decoding of conceptual representations. PloS one, 5(12).

Stam, C.J., 2005. Nonlinear dynamical analysis of EEG and MEG: review of an emerging field. *Clinical neurophysiology*, *116*(10), pp.2266-2301.

Stewart, A.X., Nuthmann, A. and Sanguinetti, G., 2014. Single-trial classification of EEG in a visual object task using ICA and machine learning. *Journal of neuroscience methods*, *228*, pp.1-14.

Taghizadeh-Sarabi, M., Daliri, M.R. and Niksirat, K.S., 2015. Decoding objects of basic categories from electroencephalographic signals using wavelet transform and support vector machines. *Brain topography*, *28*(1), pp.33-46.

Torabi, A., Jahromy, F.Z. and Daliri, M.R., 2017. Semantic category-based classification using nonlinear features and wavelet coefficients of brain signals. *Cognitive Computation*, *9*(5), pp.702-711.

Tzovara, A., Murray, M.M., Plomp, G., Herzog, M.H., Michel, C.M. and De Lucia, M., 2012. Decoding stimulus-related information from single-trial EEG responses based on voltage topographies. *Pattern Recognition*, *45*(6), pp.2109-2122.

Van Gerven, M., Farquhar, J., Schaefer, R., Vlek, R., Geuze, J., Nijholt, A., Ramsey, N., Haselager, P., Vuurpijl, L., Gielen, S. and Desain, P., 2009. The brain–computer interface cycle. *Journal of neural engineering*, *6*(4), p.041001.

Vidaurre, D., Myers, N.E., Stokes, M., Nobre, A.C. and Woolrich, M.W., 2019. Temporally unconstrained decoding reveals consistent but time-varying stages of stimulus processing. Cerebral Cortex, 29(2), pp.863-874.

Wang, C., Xiong, S., Hu, X., Yao, L. and Zhang, J., 2012. Combining features from ERP components in single-trial EEG for discriminating four-category visual objects. *Journal of neural engineering*, *9*(5), p.056013.

Wang, Y., Wang, P. and Yu, Y., 2018. Decoding English alphabet letters using EEG phase information. *Frontiers in neuroscience*, *12*, p.62.

Watrous, A.J., Deuker, L., Fell, J. and Axmacher, N., 2015. Phase-amplitude coupling supports phase coding in human ECoG. Elife, 4, p.e07886.

Williams, M.A., Dang, S. and Kanwisher, N.G., 2007. Only some spatial patterns of fMRI response are read out in task performance. *Nature neuroscience*, *10*(6), pp.685-686.

Woolgar, A., Dermody, N., Afshar, S., Williams, M.A. and Rich, A.N., 2019. Meaningful patterns of information in the brain revealed through analysis of errors. *bioRxiv*, p.673681.

Zellner, A. and Siow, A., 1980. Posterior odds ratios for selected regression hypotheses. *Trabajos de estadística y de investigación operativa*, *31*(1), pp.585-603.